The Use of Ternary Cations to Control Nucleation: Avoiding Binary Compounds as Reaction Intermediates

Robert Schneidmiller, Anne Bentley, Marc D. Hornbostel, and David C. Johnson*

Contribution from the Department of Chemistry and Material Science Institute, University of Oregon, Eugene, Oregon 97403

Received September 24, 1998

Abstract: In this article we compare and contrast the evolution of ternary modulated reactants of the form M−Mo−Se (M = Ni, Zn, Sn, In, and Cu) with each other and with the binary Mo−Se system. The binary elementally modulated reactants interfacially nucleate $MoSe_2$ over a broad composition range surrounding that of the binary compound Mo_6Se_8. Increasing the concentration of any of the studied ternary elements except nickel above a critical value in the initial reactant suppressed interfacial nucleation of the diselenide. The nickel-containing reactants all interfacially nucleated Ni_xMoSe_2 at low temperatures. The subsequent nucleation and growth of crystalline compounds from the amorphous intermediates obtained in the other four systems was found to depend on both the identity and concentration of the ternary element. In the Sn−Mo−Se system, a layered dichalcogenide was the first compound nucleated. In the Zn−Mo−Se system, the dichalcogenide and the ternary compound $Zn_xMo_6Se_8$ were observed to nucleate at approximately the same temperature. In the copper- and indium-containing systems, the cluster-containing compounds, $Cu_xMo_6Se_8$ and $In_{3.33\pm\delta}Mo_{15}Se_{19}$, were observed to be the first crystalline compounds formed. Annealing all four of these systems at temperatures greater than 1100 °C resulted in the growth of Chevrel phase compounds at the expense of molybdenum diselenide.

Introduction

The traditional distinction between organic and inorganic chemistry has a historical basis which has become less well defined as organometallic chemistry and reagents have been developed. As suggested by others,[1] a potentially more meaningful division would be to divide the subject into molecular chemistry and solid-state chemistry, the chemistry of extended structures. These two areas have had distinctly different synthetic approaches. Although molecular chemistry has focused on reaction mechanisms and controlling reaction kinetics, these concepts are not well developed in solid-state chemistry. This difference results from the vastly different diffusion rates found in the traditional solutions used in molecular synthesis versus the solid-state processes that occur in traditional solid-state synthesis. The many orders of magnitude slower diffusion rates found between typical solid-state reactants used to prepare extended inorganic solids has forced solid-state chemists to use very high reaction temperatures.[2] This, for the most part, limits the products to the thermodynamically most stable compounds. Many important aspects of the chemistry are undoubtedly lost by the use of such high reaction temperatures.[3] As a rule, all compounds stable at low temperature are inaccessible as well as compounds that are thermodynamically unstable. In addition, the lack of knowledge of the reaction mechanism prevents full exploitation of the synthesis conditions.

To overcome some of these limitations, we have developed a synthesis method that uses elementally modulated superlattices as the initial reactants. The elementally modulated reactants are made by sequentially depositing, in high vacuum, thin layers

(5−20 Å) of reactants.[4] The hypothesis is that the composition and structure of the initial modulation can be used to control the kinetics of the subsequent interdiffusion and crystallization. By controlling the kinetics, we hope to gain access to metastable compounds as well as compounds only stable at low temperatures. Important to these goals is the ability to follow the course of the interdiffusion reactions occurring at the interfaces. The modulated structure of the initial reactant results in a diffraction pattern that contains information on the spatial extent of interdiffusion as well as roughness of the interfaces.[5,6] The evolution of this diffraction pattern as a function of temperature and time permits the interfacial reactions to be followed to an extent not previously possible.[7] The sensitivity of the diffraction pattern to compositional changes permits interdiffusion rates as small as 10^{-27} cm^2/s to be followed.[8] The short diffusion distances make these small interdiffusion rates synthetically important and meaningful. Indeed, this synthetic approach takes advantage of the slow diffusion rates of atoms in solids to kinetically trap metastable structures. The short diffusion distances also permit the reaction progress to be observed with use of differential scanning calorimetry. Exotherms are typically observed during the mixing of the elemental layers as well as during the nucleation and subsequent growth of crystalline compounds. If the initial layer thicknesses are thin enough, the rate-limiting step in crystalline product formation is nucleation.[9]

(1) Schon, J. C.; Jansen, M. *Angew. Chem., Int. Ed. Engl.* **1996,** *35,* 1286.
(2) DiSalvo, F. J. *Science* **1990,** *247,* 649−655.
(3) Brewer, L. *J. Chem. Educ.* **1958,** *35,* 153.

(4) Fister, L.; Li, X. M.; Novet, T.; McConnell, J.; Johnson, D. C. *J. Vac. Sci., Technol. A* **1993,** *11,* 3014−3019.
(5) Xu, Z.; Tang, Z.; Kevan, S. D.; Novet, T.; Johnson, D. C. *J. Appl. Phys.* **1993,** *74,* 905−912.
(6) Greer, A. L.; Spaepen, F. *Diffusion*; Chang, L. C., Giessen, B. C., Eds.; Academic Press: New York, 1985; pp 419−486.
(7) Novet, T.; McConnell, J. M.; Johnson, D. C. *Chem. Mater.* **1992,** *4,* 473−478.
(8) Greer, A. L. *Curr. Opin. Solid State Mater. Sci.* **1997,** *2,* 300−304.
(9) Novet, T.; Johnson, D. C. *J. Am. Chem. Soc.* **1991,** *113,* 3398−3403.

Although this synthesis approach has shown considerable promise,[10] approaches need to be developed to control the nucleation process if the compound desired is not naturally the easiest to nucleate. The binary molybdenum−selenium system provides an illustration of a system in which control of nucleation would be desired.[11] In this binary system, it is difficult to avoid interfacial nucleation of $MoSe_2$ over a wide range of composition. Low-temperature synthesis using elementally modulated reactants produced a new compound, Mo_3Se, which is only stable at low temperatures. This approach did not, however, result in the direct nucleation of the desired thermodynamically stable compound, Mo_6Se_8, from an amorphous intermediate. Mo_6Se_8 was formed only through extended annealing at high temperatures. We believe that direct nucleation of Mo_6Se_8 does not occur in the molybdenum−selenium system because of the complexity of its cluster structure relative to the structures of $MoSe_2$ and Mo_3Se. The local coordination of the molybdenum in the amorphous alloy is likely to be either octahedral or tetrahedral depending on composition. Nucleation of $MoSe_2$ and Mo_3Se involves local rearrangements of the amorphous intermediate, whereas forming the octahedral Mo_6 clusters found in Mo_6Se_8 requires considerably larger changes in coordination geometries of the atoms.

The crystal chemistry of the stable compound Mo_6Se_8 and the competing binary $MoSe_2$ provides an interesting opportunity, however, to explore the effect of composition on nucleation. $M_xMo_6Se_8$ compounds can be made over the range $0 < x < 4$ for elements with small M cations but only at $x = 1$ for large elements.[12,13] For most elements M, $MoSe_2$ cannot be intercalated to form M_xMoSe_2 compounds.[14] Therefore, we can use this as a model system to study the effect of adding a ternary element to disrupt the formation of binary compounds. This article addresses whether we can avoid nucleating the binary compound $MoSe_2$ by adding a ternary element and whether we can also lower the nucleation barrier for the cluster compound by adding a ternary element. This issue has recently been addressed theoretically by Desré who showed that an increase in the number of components in a liquid glass forming alloy inhibits nucleation.[15] The ternary element is an additional component with respect to nucleation of $MoSe_2$, whereas it is not an additional component with respect to the nucleation of $M'Mo_6Se_8$. By using a variety of ternary elements, we also address the effect of ternary cation size and valence on the evolution of the reactants.

Experimental Section

Approximately 90 multilayer samples were prepared in a high-vacuum evaporation system which has been described in detail elsewhere.[4] The elements were deposited sequentially in high vacuum (approximately 5×10^{-7} Torr) under the control of a personal computer. The elements were deposited from electron beam evaporation sources at a rate of 0.5 Å/s. Each source was monitored independently by quartz crystal thickness monitors. The thickness of each elemental layer was controlled to better than an angstrom. This control is limited by random rate fluctuations, the thermal time constant of the deposition source, and the time constant of the feedback. Intended thicknesses were inputted to a tenth of an angstrom, which reflects the smaller deviation of the mean thickness of a given layer in a multilayer reactant from

(10) Murphy, D. W.; West, A. R. *Curr. Opin. Solid State Mater. Sci.* **1998**, *3*, 125−127.

(11) Schneidmiller, R.; Hornbostel, M. D.; Johnson, D. C. *Inorg. Chem.* **1997**, *36*, 5894−5899.

(12) Yvon, K. *Curr. Top. Mater. Sci.* **1979**, *3*, 1−53.

(13) Fischer, O. *Appl. Phys.* **1978**, *16*, 1.

(14) Liang, W. Y. *Intercalation in Layered Materials*; Dresselhaus, M. S., Ed.; Plenum Press: New York, 1986.

(15) Desré, P. J. *Mater. Trans. JIM* **1997**, *38*, 583−588.

Table 1. A Summary of the Ni−Mo−Se Multilayer Samples Prepared as Part of This Investigation

	intended					low-angle XRD (Å)	compositional analysis
sample	Mo (Å)	Ni (Å)	Se (Å)	Ni (Å)	total Å		
Ni-1	4.4		9.2	0.9	14.5	13.8	$Ni_{2.9}Mo_6Se_{7.6}$
Ni-2	4.6	0.3	9.2	0.3	14.4	14.02	$Ni_{4.5}Mo_6Se_{8.4}$
Ni-3	4.7	0	9.2	0.9	14.8	14.11	$Ni_{4.8}Mo_6Se_{7.7}$
Ni-4	4.8	0.4	9.2	0.4	14.8	15.18	$Ni_{6.6}Mo_6Se_{6.9}$
Ni-5	4.6	0.4	9.2	0.4	14.6	14.07	$Ni_{6.9}Mo_6Se_{8.1}$
Ni-6	4.3	0	9.2	0.4	13.9	14.3	$Ni_{6.9}Mo_6Se_{8.2}$
Ni-7	4.6	0.5	9.2	0.5	14.8	15.47	$Ni_{7.0}Mo_6Se_{8.3}$
Ni-8	4.6	0.5	9.2	0.5	14.8	14.34	$Ni_{7.4}Mo_6Se_{8.8}$
Ni-9	4.6	0.4	9.2	0.4	14.6	14.83	$Ni_{8.8}Mo_6Se_{8.9}$
Ni-10	4.6	0.6	9.2	0.6	15.0		$Ni_{9.4}Mo_6Se_{7.8}$
Ni-11	4.6	0.7	9.2	0.7	15.2	15.09	$Ni_{9.7}Mo_6Se_{8.6}$

the intended thickness. The proportionality or tooling factor for each deposition source (the ratio of the amount of material deposited on the sample divided by the amount of material deposited on the quartz crystal) was determined from the measured repeat thicknesses in a series of calibration samples. The films were deposited simultaneously on silicon and polymer-coated silicon wafers. The substrates were not intentionally heated during deposition. Radiation emitted by the deposition sources, however, warms the samples while the shutters are open. We estimate from the onset of interdiffusion that the sample temperatures remain below 100 °C during deposition. The silicon substrates were used for low-angle diffraction studies. The coated substrates were used to allow the sample to be removed from the substrate by soaking in acetone and collecting with poly(tetrafluoroethylene) (PTFE) filters.

Low-angle X-ray diffraction (XRD) was used to characterize the multilayer periodicity and to study the interdiffusion of the elements. For almost all the samples studied, diffraction maxima resulting from the elemental modulation were observed. High-angle XRD was used to identify crystalline compounds. Copper Kα radiation was used in the diffraction studies. The average composition of the multilayer films was determined by electron microprobe analysis using an energy-dispersive X-ray detector. Crystallinity of the samples was also examined using through-foil transmission electron microscopy (TEM) in which free-standing films were mounted on standard copper grids. The TEM used was a Phillips CM12 operated at an accelerating voltage of 100 keV.

Samples were annealed in a nitrogen atmosphere with less than 1 ppm oxygen. Substrate-free samples were annealed in a differential scanning calorimeter. Measured exotherms were correlated with X-ray and TEM results to identify and track the interdiffusion of the elements and the crystallization of any compounds.

Results and Discussion

Tables 1−5 summarize the intended elemental layer thicknesses, the measured total thickness, and the measured composition of the samples prepared in this study. Low-angle diffraction showed that the samples were layered as deposited, as shown in Figure 1. The measured total thicknesses are all close to those calculated from the intended elemental layer thicknesses. The deviations are typically within an angstrom of the intended thickness with a maximum deviation of less than 3 Å. The major source of error in the preparation of the samples is slight deviations of the position of the quartz crystal monitors during the year in which the samples were prepared. Small displacements of the crystal monitor, resulting from cleaning and crystal replacement, change the proportionality constant between the monitor and the sample. The elemental compositions of the samples with respect to the Mo−Se ratio were generally found to be repeatable to within about 5%. The errors in the amount of the ternary cation in the sample were much larger, especially for samples with a small amount of ternary metal, because we

Table 2. A Summary of the Zn−Mo−Se Multilayer Samples Prepared as Part of This Investigation

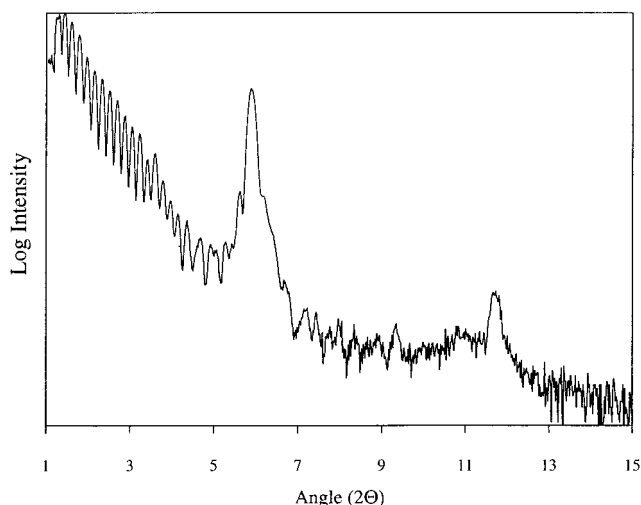| | intended | | | | | low-angle | compositional |
sample	Mo (Å)	Zn (Å)	Se (Å)	Zn (Å)	total Å	XRD (Å)	analysis
Zn-1	4.9	0.7	9.2	0.7	15.5	16.97	$Zn_{3.0}Mo_6Se_{6.9}$
Zn-2	4.2	0.7	9.2	0.7	14.8	15.3	$Zn_{3.4}Mo_6Se_{8.3}$
Zn-3	4.6	0.7	9.2	0.7	15.2	15.36	$Zn_{3.5}Mo_6Se_{7.8}$
Zn-4	4.9	1.3	9.2	1.3	16.7	15.97	$Zn_{4.2}Mo_6Se_{8.2}$
Zn-5	4.6	0	9.2	2.4	16.2	15.61	$Zn_{4.2}Mo_6Se_{8.8}$
Zn-6	4.6	0	9.2	2.0	15.8	15.66	$Zn_{4.2}Mo_6Se_{9.0}$
Zn-7	4.6	0.9	9.2	0.9	15.6	15.84	$Zn_{4.3}Mo_6Se_{8.7}$
Zn-8	4.6	1.0	9.2	1.0	15.8	16.45	$Zn_{4.5}Mo_6Se_{8.7}$
Zn-9	4.6	1.3	9.2	1.3	16.4	16.29	$Zn_{4.8}Mo_6Se_{8.2}$
Zn-10	4.2	1.0	9.2	1.0	15.4	15.92	$Zn_{4.8}Mo_6Se_{8.7}$
Zn-11	4.2	1.3	9.2	1.3	16.0	16.45	$Zn_{5.0}Mo_6Se_{9.0}$
Zn-12	4.6	1.3	9.2	1.3	16.4	15.85	$Zn_{5.3}Mo_6Se_{9.4}$

Table 3. A Summary of the Sn−Mo−Se Multilayer Samples Prepared as Part of This Investigation

| | intended | | | | low-angle | compositional |
sample	Mo (Å)	Sn (Å)	Se (Å)	total Å	XRD (Å)	analysis
Sn-1	4.6	0.2	9.2	14.0	13.2	$Sn_{0.5}Mo_6Se_{7.4}$
Sn-2	4.2	0.4	9.2	13.8	12.66	$Sn_{0.6}Mo_6Se_{7.6}$
Sn-3	4.2	0.2	9.2	13.6	12.66	$Sn_{0.6}Mo_6Se_{7.9}$
Sn-4	4.2	0.5	9.2	13.9		$Sn_{0.9}Mo_6Se_{7.4}$
Sn-5	4.2	0.6	9.2	14.0	14	$Sn_{1.0}Mo_6Se_{7.7}$
Sn-6	4.2	0.7	9.2	14.1	14.67	$Sn_{1.2}Mo_6Se_{7.5}$
Sn-7	4.2	0.9	9.2	14.3	14.44	$Sn_{1.2}Mo_6Se_{7.7}$
Sn-8	4.2	1.0	9.2	14.4	14.29	$Sn_{1.4}Mo_6Se_{7.8}$
Sn-9	4.2	1.3	9.2	14.7	14.82	$Sn_{1.9}Mo_6Se_{8.0}$
Sn-10	4.2	1.6	9.2	15.0	14.8	$Sn_{2.3}Mo_6Se_{8.2}$

Table 4. A Summary of the In−Mo−Se Multilayer Samples Prepared as Part of This Investigation

| | intended | | | | | low-angle | compositional |
sample	Mo (Å)	In (Å)	Se (Å)	In (Å)	total Å	XRD (Å)	analysis
In-1	4.9	0	9.2	1.4	15.5	14.68	$In_{1.3}Mo_6Se_{6.9}$
In-2	4.6	0	9.2	1.4	15.2	14.25	$In_{1.6}Mo_6Se_{7.8}$
In-3	4.9	0	9.2	1.8	15.9	15.41	$In_{1.7}Mo_6Se_{6.9}$
In-4	4.9	0	9.2	2.1	16.2	15.62	$In_{2.0}Mo_6Se_{6.7}$
In-5	4.6	0	9.2	1.8	15.6	14.58	$In_{2.0}Mo_6Se_{7.9}$
In-6	4.6	0	9.2	2.1	15.9	14.93	$In_{2.4}Mo_6Se_{8.3}$
In-7	4.6	1.1	9.2	1.1	16.0	16.09	$In_{2.8}Mo_6Se_{8.7}$
In-8	4.9	1.8	9.2	1.8	17.7	17.58	$In_{3.3}Mo_6Se_{7.0}$
In-9	4.6	1.8	9.2	1.8	17.4	17.3	$In_{3.4}Mo_6Se_{8.0}$
In-10	4.2	1.8	9.2	1.8	17.0	17.4	$In_{4.0}Mo_6Se_{8.1}$
In-11	4.9	2.2	9.2	2.2	18.5	18.09	$In_{4.2}Mo_6Se_{7.5}$
In-12	4.6	1.8	9.2	1.8	17.4	16.23	$In_{4.3}Mo_6Se_{8.6}$
In-13	4.9	2.7	9.2	2.7	19.5	17.94	$In_{4.6}Mo_6Se_{6.7}$
In-14	4.6	2.4	9.2	2.4	18.6	18.9	$In_{4.6}Mo_6Se_{7.4}$
In-15	4.6	2.2	9.2	2.2	18.2	16.51	$In_{4.7}Mo_6Se_{8.2}$
In-16	4.2	2.2	9.2	2.2	17.8	18.02	$In_{4.7}Mo_6Se_{8.2}$
In-17	4.6	0	9.2	4.0	17.8	16.15	$In_{5.2}Mo_6Se_{9.5}$
In-18	4.2	2.7	9.2	2.7	18.8	17.94	$In_{5.7}Mo_6Se_{8.7}$

Table 5. A Summary of the Cu−Mo−Se Multilayer Samples Prepared as Part of This Investigation

| | intended | | | | low-angle | compositional |
sample	Mo (Å)	Se (Å)	Cu (Å)	total Å	XRD (Å)	analysis
Cu-1	4.2	9.2	0.4	13.8		$Cu_{1.0}Mo_6Se_{8.6}$
Cu-2	4.2	9.2	0.1	13.5	13.44	$Cu_{1.1}Mo_6Se_8$
Cu-3	4.4	9.2	0.5	14.1	13.12	$Cu_{1.6}Mo_6Se_{7.7}$
Cu-4	4.2	9.2	0.6	14.0	13.59	$Cu_{2.0}Mo_6Se_{7.9}$
Cu-5	4.2	9.2	0.8	14.2	13.59	$Cu_{2.1}Mo_6Se_{8.2}$
Cu-6	4.2	9.2	0.7	14.1	13.65	$Cu_{2.1}Mo_6Se_{8.6}$
Cu-7	4.2	9.2	1.2	14.6	13.69	$Cu_{2.4}Mo_6Se_{8.7}$
Cu-8	4.2	9.2	0.9	14.5	13.5	$Cu_{2.5}Mo_6Se_{7.6}$
Cu-9	4.2	9.2	1.0	14.4	13.5	$Cu_{2.6}Mo_6Se_{8.8}$
Cu-10	4.2	9.2	1.4	15.0	13.8	$Cu_{2.8}Mo_6Se_{7.7}$
Cu-11	4.2	9.2	1.0	14.4	13.59	$Cu_{2.8}Mo_6Se_8$
Cu-12	4.4	9.2	1.1	14.7	13.12	$Cu_{2.9}Mo_6Se_{8.6}$
Cu-13	4.2	9.2	1.3	14.7	14.06	$Cu_{3.0}Mo_6Se_{8.3}$
Cu-14	4.2	9.2	1.6	15.0	14.39	$Cu_{3.3}Mo_6Se_{8.2}$
Cu-15	4.2	9.2	1.6	15.0	16.59	$Cu_{3.5}Mo_6Se_{8.7}$
Cu-16	4.4	9.2	1.2	14.8	14.01	$Cu_{3.7}Mo_6Se_{7.8}$
Cu-17	4.4	9.2	1.8	15.4	13.65	$Cu_{3.8}Mo_6Se_{7.7}$
Cu-18	4.4	9.2	1.4	15.0	12.93	$Cu_{3.9}Mo_6Se_{7.9}$
Cu-19	4.2	9.2	2.2	15.6	13.69	$Cu_{3.9}Mo_6Se_{9.0}$
Cu-20	4.2	9.2	2.5	15.9	15.47	$Cu_{4.4}Mo_6Se_{8.7}$
Cu-21	4.2	9.2	2.7	16.1	18.59	$Cu_{4.5}Mo_6Se_{8.7}$
Cu-22	4.2	9.2	1.9	15.3	14.85	$Cu_{4.5}Mo_6Se_{9.7}$
Cu-23	4.2	9.2	2.5	15.9	18.31	$Cu_{5.1}Mo_6Se_{9.4}$
Cu-24	4.2	9.2	1.9	15.3	16.15	$Cu_{5.2}Mo_6Se_{10.2}$
Cu-25	4.2	9.2	1.3	14.7	15.8	$Cu_{5.2}Mo_6Se_{13.0}$
Cu-26	4.2	9.2	1.0	14.4	14.29	$Cu_{5.2}Mo_6Se_{15.4}$
Cu-27	4.2	9.2	2.2	15.6	17.33	$Cu_{5.7}Mo_6Se_{8.5}$
Cu-28	4.2	9.2	3.6	17.0	16.89	$Cu_{5.7}Mo_6Se_{9.7}$
Cu-29	4.2	9.2	2.7	16.1	14.91	$Cu_{5.9}Mo_6Se_{9.2}$
Cu-30	4.2	9.2	3.3	16.7	16.44	$Cu_{6.5}Mo_6Se_{12.8}$
Cu-31	4.2	9.2	3.3	16.7	15.88	$Cu_{6.7}Mo_6Se_{10.0}$
Cu-32	4.2	9.2	3.0	16.4	17.45	$Cu_{6.8}Mo_6Se_{9.7}$
Cu-33	4.2	9.2	4.2	17.6	16.31	$Cu_{8.2}Mo_6Se_{11.5}$
Cu-34	4.2	9.2	3.0	16.4	16.44	$Cu_{8.3}Mo_6Se_{11.3}$
Cu-35	4.2	9.2	3.6	17.0	16.51	$Cu_{9.3}Mo_6Se_{13.0}$
Cu-36	4.2	9.2	3.9	17.3	16.01	$Cu_{10.2}Mo_6Se_{14.0}$

Figure 1. Low-angle X-ray diffraction pattern of Ni sample 11. Modulation of the sample is revealed by the first- and second-order Bragg diffraction maxima at roughly 6 and 12 deg, respectively.

did not get to take advantage of time averaging of the deposition rate as a result of the short time the shutter was open. The relatively high vapor pressure of selenium also contributed to a trend in the samples summarized in Tables 1−5. The combination of the sticking coefficient of selenium being less than one as well as reevaporation of the selenium in the dynamic vacuum results in selenium loss before it is buried by subsequent elemental layers. If Se can alloy during the deposition with one of the depositing elements, then the reevaporation of Se decreases because of its decreased vapor pressure. The Mo−Se interdiffusion rates are much smaller than the ternary metal−selenium interdiffusion rates so only the ternary metal is able

to interdiffuse with selenium during deposition. The tooling factor therefore changes with the amount of ternary metal evaporated. If one calculates the intended compositions using crystalline densities and the layer thicknesses of the component elements, one finds a systematic increase in the selenium content as a function of both the identity and the amount of ternary
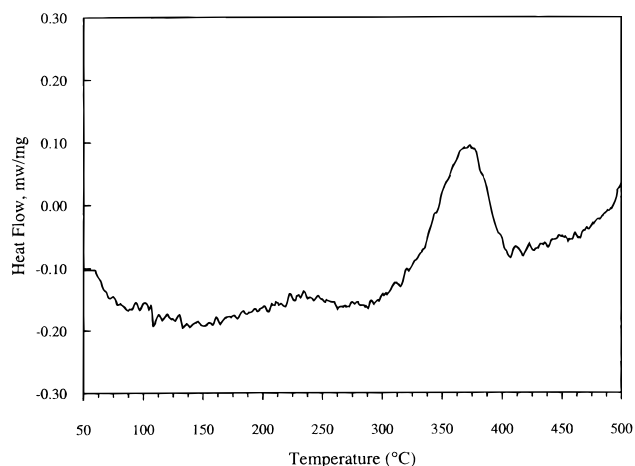
Use of Ternary Cations to Control Nucleation

J. Am. Chem. Soc., Vol. 121, No. 13, 1999 3145

Figure 2. Differential scanning calorimetry of Ni sample 3. The exotherm at 360 °C is due to crystal growth.
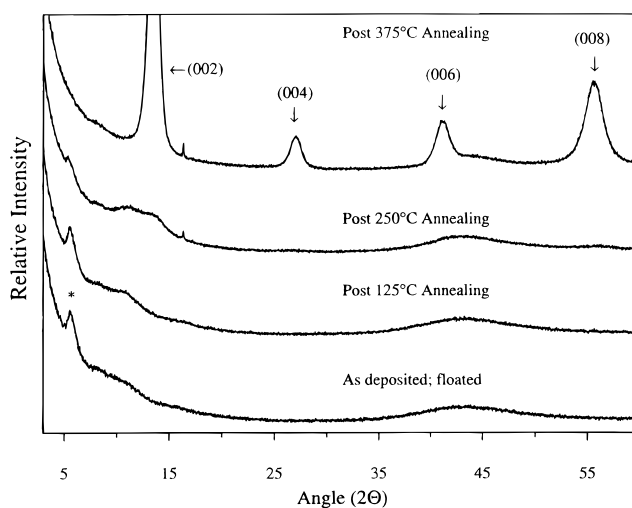

Figure 3. X-ray diffraction analysis of Ni sample 11. At 250 °C modulation ($*$) is present simultaneously with weakly diffracting dichalcogenide crystals at 12 deg. Strongly diffracting dichalcogenide crystals have grown in by 375 °C.

metal evaporated. This systematic trend is most apparent in the measured compositions of the Cu–Mo–Se reactants summarized in Table 5, because copper and selenium have the highest interdiffusion rates of all the elements studied. We do not see a systematic increase in the repeat layer thicknesses because the Cu–Se alloy has a higher density than the sum of the elemental densities.

Our primary goal in this study was to determine whether we could avoid interfacial nucleation of $MoSe_2$ at the reacting Mo–Se interface. In our study of the binary Mo–Se system, we observed interfacial nucleation of $MoSe_2$ over a broad composition range when the repeat layer thicknesses were greater than approximately 20 Å. This critical thickness was found to decrease as the samples became more molybdenum rich.[11] For ternary samples, we speculated that we potentially could take advantage of the presence of a ternary element to avoid this interfacial reaction. To test two different potential reaction sequences, we examined Ni–Mo–Se and Zn–Mo–Se. Previous investigations of binary Ni–Se and Zn–Se elementally modulated reactants showed a dramatic difference in their evolution. Zinc–selenium reactants were found to interdiffuse rapidly at low temperatures, forming an amorphous zinc–selenium alloy that was relatively stable with respect to annealing. Nickel–selenium reactants were found to form binary compounds at relatively low temperatures. For example, $NiSe_2$ was observed to form exothermically from a modulated reactant at 140 °C. If the interfaces in the ternary M–Mo–Se reactants behaved in the same manner, the zinc system would form a binary zinc–selenium alloy which would then react with Mo, whereas the nickel system would form binary nickel–selenium compounds before significant reaction with molybdenum.

A summary of the ternary Ni–Mo–Se modulated reactants prepared as part of this investigation can be found in Table 1. Differential scanning calorimetry (DSC) analysis of the samples was conducted to probe the evolution of the samples as a function of annealing temperature. Low-temperature exotherms occurred when the Ni composition, x (where x is given by the molar ratio of the elements normalized to the selenium content, i.e., $\sim$0.75:1:x), was above 0.54 (24 atom %) as shown in Figure 2. High-angle XRD data were collected on samples before and after the exothermic event as shown in Figure 3. Before the exotherm, diffraction maxima from the multilayer structure occur simultaneously with weak $MoSe_2$ diffraction maxima. Diffraction patterns of samples after their exothermic event showed well-grown and oriented $MoSe_2$ crystals. These dif-

fraction data suggest that heat released during crystal growth is the cause of the exotherm. Surprisingly, the diselenide formed has an increased c-axis lattice parameter relative to pure $MoSe_2$, suggesting that the nickel is incorporated into the diselenide structure. Samples with Ni composition, x, below 0.54 (24 atom %) also formed Ni_xMoSe_2; however, no exotherm was observed in the DSC data for these samples. No diffraction evidence for the formation of the expected binary nickel selenides was observed in any of the samples studied. The nickel does not suppress the nucleation of $MoSe_2$ because $MoSe_2$ interfacially nucleates (before nickel and selenium can appreciably interdiffuse), and nickel is also incorporated into the $MoSe_2$ structure. The nickel does not act as an additional component which, according to Desré,[15] would suppress nucleation of the dichalcogenide.

Table 2 contains a summary of the ternary Zn–Mo–Se modulated reactants prepared. Twelve samples were made with Mo:Se:Zn ratios near 0.75:1:x, with x ranging from 0.37 to 0.66. The DSC data collected on these 12 samples from room temperature to 550 °C contained no exothermic or endothermic events. Low- and high-angle diffraction studies of the samples, Figures 4 and 5, show that the layers had mixed together, but no crystalline compounds had nucleated after annealing at 550 °C. Higher temperature annealing followed by X-ray analysis shows the growth of crystalline compounds from this amorphous intermediate. The diffraction data show that the first compound to form is $Zn_xMo_6Se_8$, but it is overtaken by $MoSe_2$ crystal growth at higher temperatures. Annealing at 1250 °C in nitrogen environment reproduced the expected thermodynamically stable Chevrel phase structure.

Zinc appears to promote the formation of an amorphous intermediate by inhibiting interfacial nucleation of the diselenide. We believe suppression of diselenide formation is the result of the ability of zinc to interdiffuse readily with Se before interfacial nucleation between Mo and Se can occur. High zinc–selenium diffusion rates at low temperatures permit zinc to diffuse evenly throughout the Se layer before significant interdiffusion of molybdenum. This is shown schematically in Figure 6. The formation of this homogeneous Zn–Se amorphous alloy inhibits interfacial nucleation of the $MoSe_2$ because the zinc atoms disrupt the formation of the Mo–Se bonds required to form $MoSe_2$. Most of the zinc needs to be removed from the volume of a critical nucleus before $MoSe_2$ can nucleate. A
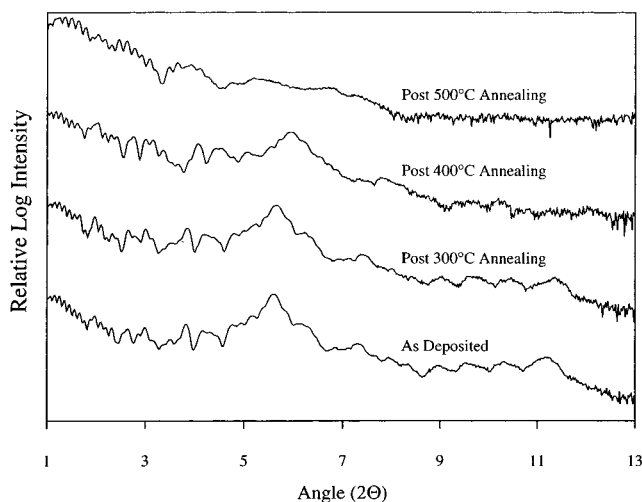
Figure 4. Low-angle diffraction data collected as a function of annealing time and temperature on Zn sample 7. The diffraction maxima at 5.5 and 11 deg are the first- and second-order Bragg diffraction maxima resulting from the modulation in the as-deposited form. These diffraction maxima degrade with increasing temperature and are gone by 500 °C, indicating the sample is no longer modulated.
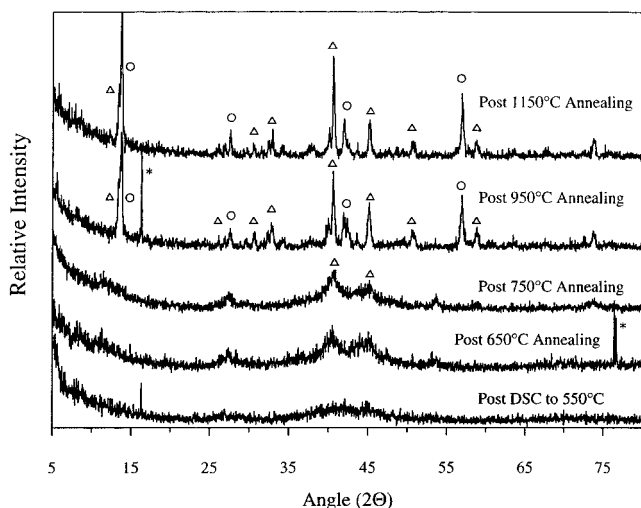

Figure 5. Diffraction data collected as a function of annealing time and temperature on sample Zn 1. The sample is X-ray amorphous after heating to 550 °C. Further annealing results first in the growth of poorly crystalline $Zn_xMo_6Se_8$ ($\triangle$) which is followed by the growth of $MoSe_2$ ($\bigcirc$). The maxima at 16 deg and 76 deg ($\ast$) were not identified.

Figure 6. A schematic comparison of diffusion routes of the binary Mo−Se and ternary M−Mo−Se systems. In the ternary Zn−Mo−Se system shown in the top schematic, the Zn and Se layers in the modulated reactant interdiffuse first before reacting with the molybdenum layer. The ternary product, $Zn_xMo_zSe_y$ can be either amorphous or crystalline depending on Zn concentration, annealing temperatures, and annealing times.

critical concentration of zinc is required to suppress $MoSe_2$ nucleation which must be between the values of 0 and 0.37 studied as part of this investigation. At higher temperatures,
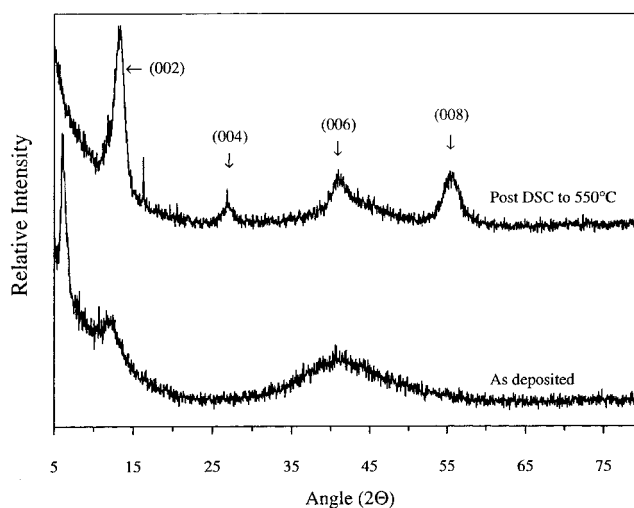

Figure 7. Diffraction data collected as deposited and after DSC analysis of Sn sample 5. The as-deposited spectrum shows both modulation and weak crystalline diffraction maxima at 7 and 12 deg, respectively, revealing interfacial nucleation has occurred. The top spectrum shows the (00l) peaks of $MoSe_2$.

diffusion between the Zn−Se alloy and Mo occurs to give an amorphous ternary intermediate, whose composition is near that of the intended Chevrel phase. Composition should then control the compound nucleated from the intermediate. The diffraction data collected as a function of annealing temperature and time shows that the incorporation of zinc in the amorphous intermediate suppresses diselenide nucleation. At higher annealing temperatures ($\sim$800 °C), however, the diselenide nucleates and grows at a faster rate than the desired Chevrel phase. The low-temperature growth and subsequent decomposition of a Chevrel phase structure was observed previously by Schewe-Miller et al. studying the formation kinetics of $PbMo_6S_8$ from a co-deposited reactant.[16]

The Mo−Se−Zn system suggests that ternary elements with relatively fast interdiffusion rates with Se are a key to promoting the formation of the Chevrel phases by delaying and/or bypassing the nucleation of molybdenum diselenide. The ternary element must interdiffuse into the Se layer at a temperature below that which results in interfacial nucleation between Mo and Se. To follow up on this hypothesis, we investigated the reaction of other ternary metal−Mo−Se reactants. Tin, indium, and copper were chosen, based on their ability to readily interdiffuse with selenium at temperatures below that required to interfacially nucleate $MoSe_2$.

The reactivity of Sn−Mo−Se reactants contains two complications not present in the zinc system. First, the Chevrel phase formed with tin, $Sn_xMo_6Se_8$, only forms in a limited composition regime about $x = 1$. Second, tin and selenium can form a layered compound, $SnSe_2$, which is structurally closely related to $MoSe_2$. To explore the kinetics of nucleation of Sn−Mo−Se reactants, 10 samples, summarized in Table 3, were made with Mo:Se:Sn ratios near 0.75:1:x, where $x = 0.04-0.28$. DSC analysis showed that no heat-flow events were observed on annealing any of the samples to 550 °C. XRD analysis revealed that samples with a lower Sn content (samples Sn-1 through Sn-5) nucleated $MoSe_2$. The diffraction studies as a function of annealing temperature suggest that these samples interfacially nucleate the diselenide structure as shown in Figure 7. Samples with a high tin content (samples Sn-9 and Sn-10) appeared to

(16) Schewe-Miller, I. M.; Li, F.; Columbia, M.; Schrader, G. L.; Franzen, H. F. *J. Alloys Compd.* **1994**, *204*, L13−L15.
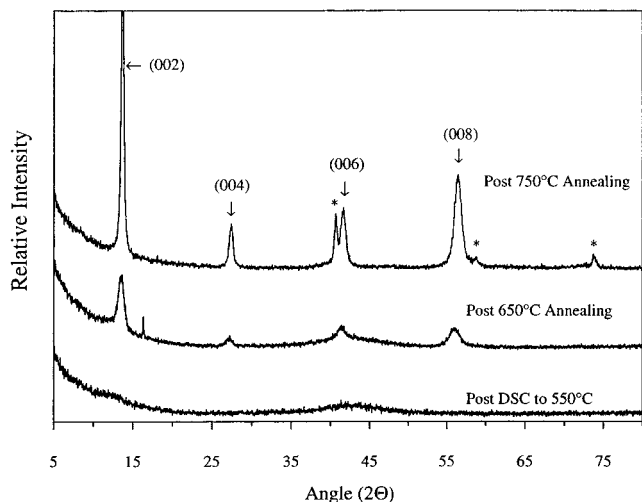
Figure 8. Diffraction data collected as a function of annealing time and temperature on Sn-rich sample 6. The sample is X-ray amorphous after DSC analysis to 550 °C. Further annealing shows the appearance of the (00*l*) peaks of the dichalcogenide. Molybdenum (∗) is also present at 750 °C.
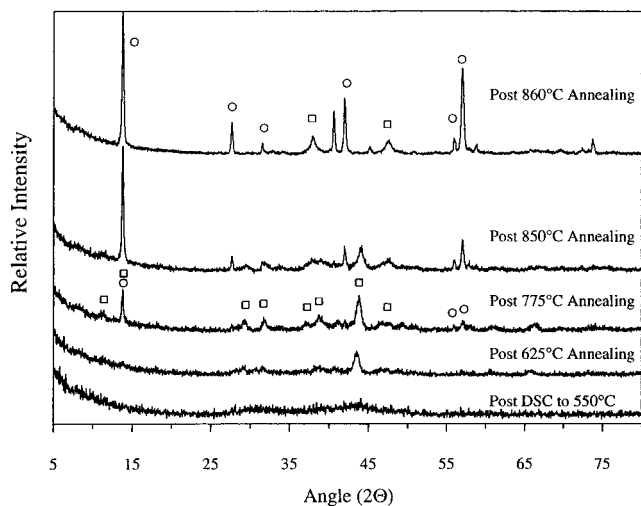

Figure 9. Diffraction data collected as a function of annealing time and temperature on In sample 15. The sample is X-ray amorphous after DSC analysis to 550 °C. Annealing to 625 °C results in the appearance of $In_xMo_{15}Se_{19}$ (□). Annealing at 775 °C results in further growth of $In_xMo_{15}Se_{19}$ (□) and the appearance of $MoSe_2$ (○). Annealing at higher temperatures results in the growth of $MoSe_2$ at the expense of $In_xMo_{15}Se_{19}$.

interdiffuse forming an amorphous intermediate. $MoSe_2$ interfacially nucleated in two of the three intermediate compositions (Sn-7 and Sn-8), whereas sample Sn-6 formed an amorphous intermediate on annealing to 550 °C. When the three amorphous samples (Sn-6, Sn-9, and Sn-10) were annealed at higher temperatures, the XRD data, shown in Figure 8, reveal the formation of $MoSe_2$. Annealing any of the samples that formed diselenide as a reaction intermediate at 1250 °C in a nitrogen atmosphere produced $Sn_xMo_6Se_8$ as expected from the Sn−Mo−Se phase diagram.

The reactivity of In−Mo−Se modulated elemental reactants was explored by preparing 18 samples with Mo:Se:In ratios near 0.75:1:*x*, where *x* = 0.16−0.71 as summarized in Table 4. Indium differs from the other ternary metals in this study by reacting with molybdenum and selenium to form several related cluster structures. In addition to the compound $InMo_6Se_8$, several compounds of stoichiometry $In_xMo_{15}Se_{19}$ can be prepared directly from the elements. The compounds $In_xMo_{15}Se_{19}$ contain Mo_9Se_{11} as well as Mo_6Se_8 clusters with a different stacking of these clusters depending on the amount of indium.[17] DSC analysis showed that no heat-flow events were observed for any of the samples, and XRD analysis of the post DSC to 550 °C samples showed that samples with a minimum In:Se ratio of 0.36:1 always produced amorphous samples. Samples with In:Se ratios less than this occasionally nucleated $MoSe_2$, whereas other samples remained amorphous. We were unable to find an experimental parameter that correlated with the nucleation of $MoSe_2$. Figure 9 summarizes a diffraction study as a function of annealing temperature. Increasing the annealing temperature of the amorphous samples resulted in the nucleation and growth of the extended Chevrel phase structure, $In_{3.3}Mo_{15}Se_{19}$. Extended annealing between 600 and 700 °C produced single-phase $In_{3.3}Mo_{15}Se_{19}$ with larger crystallites. Higher temperature annealing of these samples resulted in the formation of $MoSe_2$. Extended annealing at 1050 °C in an evacuated sealed quartz ampule produced $In_xMo_6Se_8$.

The reactivity of Cu−Mo−Se modulated elemental reactants was explored because the copper phase, $Cu_yMo_6Se_8$, forms over a wide composition range (from *y* = 0 to 3.6). The first question

(17) Chevrel, R.; Sergent, M.; Seeber, B.; Fischer, O.; Gruttner, A.; Yvon, K. *Mater. Res. Bull.* **1979**, *14*, 567.
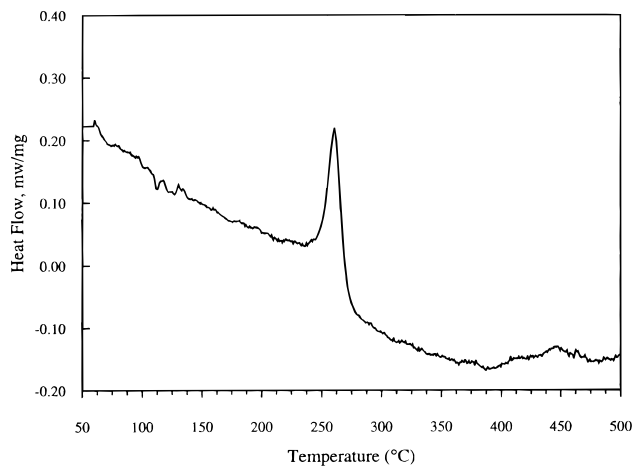

Figure 10. Representative DSC data for copper samples producing exotherms around 250 °C.

addressed was the copper concentration required to suppress the interfacial nucleation of $MoSe_2$. Thirty-six samples were made with the Mo:Se:Cu ratio of 0.75:1:*x*, where *x* = 0.12−0.89 as summarized in Table 5. DSC analysis showed that most samples with a Cu:Se ratio greater than 0.31:1 gave exotherms at about 250 °C, an example of which is shown in Figure 10. Low-angle diffraction studies as a function of annealing temperature and time, Figure 11, showed the gradual disappearance of the low-angle diffraction maxima. The low-angle diffraction maxima were still present after the nucleation exotherm. High-angle XRD analysis of the post-DSC to 550 °C samples showed that samples with a Cu:Se ratio below 0.31:1 contained primarily $MoSe_2$. Samples above this composition ratio did not contain $MoSe_2$, having only very broad and weak diffraction maxima (see Figure 12). The lack of diffraction maxima after the irreversible exotherms led us to use TEM to determine whether the samples had crystallized. The TEM data showed that the vast majority of the samples consisted of nanocrystalline $Cu_yMo_6Se_8$. XRD analysis of samples annealed at higher temperatures showed the growth of $MoSe_2$ followed by the growth the Chevrel phase at even higher temperatures
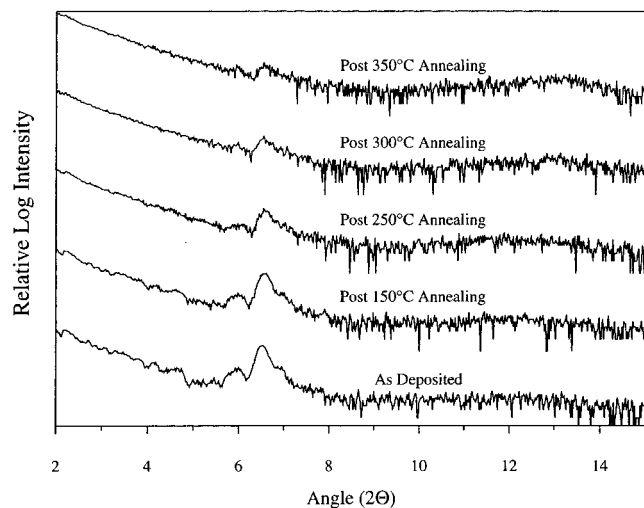
Figure 11. Low-angle diffraction data collected as a function of annealing time and temperature on Cu sample 9. The first-order Bragg diffraction maxima resulting from the modulation of the sample is seen at 6.5 deg in the as-deposited state. Annealing of the sample results in interdiffusion of the layers in the sample and the gradual decrease in the intensity of the diffraction peak because of the elemental modulation.
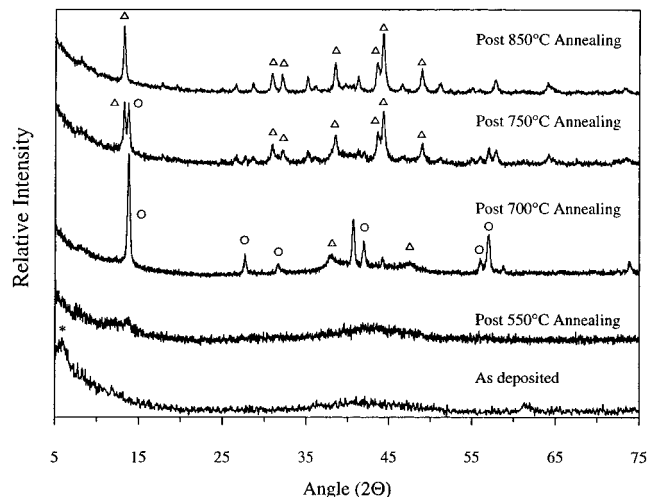

Figure 12. Diffraction data collected as a function of annealing time and temperature on Cu sample 10. Confirmation of the elemental modulation of the sample is obtained from the diffraction maxima at 6 deg (∗). The sample is essentially X-ray amorphous after annealing to 550 °C. Annealing to 700 °C produces the dichalcogenide as seen by the (00*l*) diffraction maxima (○) and the appearance of $Cu_xMo_6Se_8$ (△). Higher temperature annealing produces $Cu_xMo_6Se_8$ (△) with the disappearance of $MoSe_2$ by 850 °C.

(see Figure 12). Increasing the copper concentration further depresses nucleation of the diselenide, with the Chevrel phase being the only crystalline compound on annealing to 850 °C.

Summary

In elementally modulated Mo−Se reactants, the binary compound $MoSe_2$ interfacially nucleates at 200 °C.[11] The results presented in this article clearly demonstrate that adding a third element to the initial modulated reactant suppresses interfacial nucleation of $MoSe_2$ if the added element interdiffuses with the selenium below the temperature where interfacial nucleation of $MoSe_2$ occurs. The Cu−Mo−Se and Ni−Mo−Se modulated reactants behaved differently than the other ternary modulated reactants studied in having low-temperature exotherms. The compound formed during the exothermic reaction in the nickel-
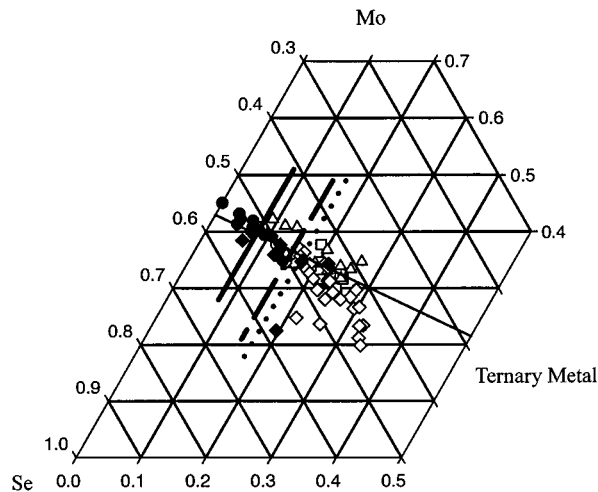

Figure 13. Ternary composition diagram of samples produced in this study distinguishing between the samples that crystallized $MoSe_2$ before interdiffusing and the samples that formed an amorphous intermediate after interdiffusion. Minimum concentrations of the ternary metals needed to produce amorphous intermediates were determined for three of the systems investigated; Sn, solid line at 8 atom % tin; Cu, dashed line at 15 atom % copper; and In, dotted line at 17 atom % indium. [○, amorphous Sn samples; ●, nonamorphous Sn samples; □, amorphous Zn samples; △, amorphous In samples; ▲, nonamorphous In samples; ◇, amorphous Cu samples; ◆, nonamorphous Cu samples.]

containing system was Ni_xMoSe_2. We believe this is a result of comparable interdiffusion rates of nickel and molybdenum with selenium. Nanocrystalline $Cu_xMo_6Se_8$ was formed in the copper-containing modulated reactants which had the low-temperature exotherm. For Zn, Sn, In, and Cu, increasing the concentration of the ternary atom relative to Mo and Se resulted in the formation of an amorphous intermediate. This is summarized in the ternary composition diagram shown in Figure 13, where the critical concentration of ternary atoms necessary to suppress nucleation of $MoSe_2$ is shown for each ternary metal. These data agree well with the theoretical work of Desré, who used a stochastic approach to show that increasing the number of components in a system lowers the probability of creating a nucleant fluctuation by a factor of 10 for each additional component added.[15] In the tin system, $MoSe_2$ was observed to initially form as small crystallites from the amorphous intermediate which subsequently reacts with the rest of the sample to form $SnMo_6Se_8$ on high-temperature annealing. In the Zn−Mo−Se system, nucleation of the ternary compound occurs simultaneously with nucleation of $MoSe_2$. In the Cu−Mo−Se system and the In−Mo−Se system, cluster compounds are the initial crystalline compound nucleated. In all the systems studied, crystal growth of the diselenide appears to be more rapid than crystal growth of the ternary compounds in the temperature range from 850 to 1000 °C. Above 1100 °C, the ternary compound grows at the expense of the diselenide. Previous work by Schewe-Miller et al. in the $PbMo_6S_8$ system on co-deposited films shows a similar behavior, with formation of $PbMo_6S_8$ at 450 °C followed by its decomposition at 550 °C.[16]

With elementally modulated reactants, repeat layer thicknesses and composition are two reaction variables that can be used to control the kinetics of phase formation to access amorphous intermediates. The results presented in this article demonstrate that further understanding of the nucleation process is required to control the subsequent nucleation and growth of crystalline compounds from amorphous intermediates. An interesting area of future investigation will be to study if techniques used in solution-phase crystallization, such as seeding with crystallites

that are isostructural to a desired structure, can be used to advantage in the crystallization of amorphous intermediates.

JA983405G